Fluid Dynamic Simulation of O_3 Decomposition in a Bubbling Fluidized Bed

Madhava Syamlal
Fluent, Inc., Morgantown, WV 26505

Thomas J. O'Brien
National Energy Technology Laboratory, Morgantown, WV 26507

Recent advances in dense, multiphase, computational fluid dynamics (CFD) have allowed accurate simulation of the gas and particle motion in bubbling and circulating fluidized beds. Since fluidized-bed reactors are used for many chemical processes, a simulation must also be able to accurately couple chemical reactions to bed hydrodynamics. The catalytic decomposition of ozone (O_3) often has been used to study experimentally the contacting behavior of catalytic reactors. Simulations of laboratory-scale experiments of premixed O_3 decomposition in a bubbling fluidized bed using the multiphase CFD code MFIX were conducted. The grid-independent results are in very good agreement with reported experimental data on total conversion over a range of fluidization velocities and initial bed heights. This confirms the ability of multiphase hydrodynamic models to capture quantitatively the effect of hydrodynamics on chemical reactions in a bubbling fluidized bed.

Introduction

Fluidized catalyst beds have better heat transfer and ease of solids handling than fixed beds. However, at a given flow velocity, the conversion in a fluidized bed is lower than in a fixed bed; the less efficient solids contacting is a result of bypassing associated with bubbles. Since the design of a fluidized-bed process is a compromise between these competing effects, the degree of contacting in any particular configuration must be quantified.

In recent years, methods of simulating the detailed behavior of bubbling fluidized beds have been developed, based on concepts of dense, multiphase, computational fluid dynamics (CFD) (Anderson and Jackson, 1967; Gidaspow, 1994). Using these methods, simulations of a bubbling bed's hydrodynamic behavior have been reported (Syamlal and O'Brien, 1985; Kuipers et al., 1992; Boemer et al., 1998; van Wachem et al., 1998; Guenther and Syamlal, 2001). Such calculations provide detailed information on the transient gas–solids flow patterns in these beds. However, in designing fluid-bed chemical reactors, simulations must also accurately describe mixing, chemical reactions, and heat transfer. Thus, previous computational studies need to be extended to include these phenomena. This has been done for circulating fluidized beds (Samuelsberg and Hjertager, 1995; Theologos and Markatos, 1993; Gidaspow and Therdthianwong, 1993). Although these simulations show qualitatively reasonable results, none of these previous studies demonstrate quantitative agreement between experimental data and grid-independent simulation results. This article reports on a study that couples chemical reactions to the hydrodynamic behavior of a bubbling fluidized bed, and provides quantified agreement with experimental results.

The ozone (O_3) decomposition reaction, catalyzed by Fe_2O_3, has become a surrogate reaction for chemical-reactor-design analysis. Although this process has no commercial applications, it has been frequently used to characterize fluidized-bed reactors, specifically to quantify gas–solids contacting (Frye et al., 1958; van Swaaij and Zuiderweg, 1972; Orcutt et al., 1962; Hovmand et al., 1971; Fryer and Potter, 1976; Ouyang et al., 1993). This reaction requires only low concentrations of the reactant, detection is rapid and accurate (using fairly simple methods), and there is a measurable reaction rate at ambient temperature and pressure (Frye et al., 1958). Moreover, since these studies have been performed with premixed O_3 at very low concentrations, density and temperature changes that occur because of the reaction can be neglected. Low concentrations also guarantee that the reaction is essentially irreversible. Being premixed, there are

Correspondence concerning this article should be addressed to M. Syamlal.

no issues of gas-phase reactant or product mixing. Thus the effect of gas–solids contacting on the chemical reaction is isolated in these experiments. For these same reasons, simulations of the O_3 decomposition reaction are used here to validate the coupling of chemistry and gas–solids hydrodynamics.

From studies on packed beds of silica sand impregnated with Fe_2O_3, O_3 decomposition has been determined to be first order in O_3 concentration and first order in Fe_2O_3 catalyst surface area (Frye et al., 1958; Orcutt et al., 1962; Fryer and Potter, 1976). The reaction rate constant is independent of the flow rate or conversion level. The reported activation energy, about 126 kJ/mol, is consistent with a surface rate-controlled reaction. Based on this work, the reaction scheme in the present simulation is described as a simple, one-step reaction, $2\ O_3 \rightarrow 3\ O_2$, catalyzed by ferric oxide, Fe_2O_3. The gas phase O_3 thermal decomposition reaction is known to occur through a chain-reaction scheme involving the atomic O free radical, and a homogeneous gas-phase scheme has been described in detail (Heimerl and Coffee, 1980). However, this reaction mechanism cannot be applied directly to catalytic decomposition in fluidized beds, since the important effects of the particulate phase, such as radical quenching on the particle surfaces, have not been accounted for. In this study, we used an empirical global reaction rate expression.

There also have been several attempts to analyze the experimental results for O_3 decomposition in fluidized beds using traditional simulation techniques. Van Swaaij and Zuiderweg (1972) interpreted their experiments using the model developed by van Deemter (1961), based on a two-phase model of fluidized beds that allows axial diffusion in the dense phase. The assumptions include: no solids in the bubble phase, plug flow in the bubble phase, negligible dense-phase gas through-flow, and eddy diffusion mixing in the dense phase. The authors concluded that the mass transfer between the bubbles and the dense phase limited conversion. Fryer and Potter (1972) developed a "back-mixing" model to account for the experimentally observed reverse flow of gases, which causes the O_3 concentration to pass through a minimum value within the reactor. Later, Bukur (1978) showed a weakness of the back-mixing model: near the conditions of flow reversal, the model predicts that the cross-sectional area of the bubble and its cloud exceeds the cross-sectional area of the bed. Peters et al. (1982) developed a model by dividing the fluidized bed into a number of axial compartments, each consisting of bubble, cloud, and emulsion phases. In their report, the compartment sizes varied from 0.5 cm to 10 cm, and the number of compartments varied from 5 to 25. The model contains several parameters that characterize fluidization: superficial gas velocity in bubble, cloud and emulsion phases, volume ratio between cloud and bubble phases, bubble diameter, number of bubbles per compartment, volume fraction of each phase, expanded bed height, gas interchange coefficient, and crossflows. The authors used empirical correlations to calculate the parameters and obtained excellent agreement between the experimental data and model predictions.

For the model described in this article, the only empirical information about the fluidized bed needed is the easily determined minimum fluidization velocity. The formation and behavior of the bubble, cloud, and emulsion phases are predicted by solving the momentum and continuity (hydrodynamic) equations. The effect of these phases on the chemical reactions is described by solving the species mass-balance equations, coupled with the hydrodynamic equations. The advantage of this approach, once validated, is its ability to describe fluidized beds of any size or configuration without recalibrating the model. The disadvantage, however, is the significantly higher computational cost. This article addresses the validation issue.

Fryer and Potter Experimental Facility

The operating conditions and hydrodynamic and chemical behavior of the experimental facility must be known for a validation study. The experimental report of Fryer and Potter (1976) provides the most detailed information over the broadest range of operating parameters. Their experimental apparatus was a cylindrical 200-$\times$ 22.9-cm dia. stainless steel and glass reactor with a bubble-cap distributor, a plate with 61 caps at 27.8-mm spacing. The bed was fluidized with dry air (since the reaction is extremely sensitive to water-vapor concentration at room temperature), to which a small amount of O_3 was added. The bed material was sand impregnated with iron oxide as a catalyst. The reactivity of the catalyst was determined by measurements in a fixed bed. The simulation conditions are listed in Table 1; some parameters were specified in the experimental article and others were deduced as discussed below.

Parameters not specified by Fryer and Potter (labeled "Other Assumed Parameters" in Table 1) were obtained as follows: the sphericity of 0.75 was obtained from figure 1 in Kunii and Levenspiel (1991) for the void fraction, ϵ_{mf}. The reported U_{mf} was used to determine parameters c and d in the drag formula. This ensures that the drag formula gives the experimentally observed drag force at the minimum fluidization condition. The coefficient of restitution ("Viscous Regime" Table 2) was chosen as 0.8, which is a typical value for the sand used in the experiment. Furthermore, the simulation results are not sensitive within a typical range of this value, because the dominant forces in a bubbling bed are the drag and gravitational forces (for example, see van Wachem et al., 2001). The angle of internal friction ("Plastic Regime," Table 2) is important for predicting a freely bubbling state

Table 1. Simulation Conditions

Reported by Fryer and Potter (1976)		
Particle diameter, d_p	117	μm
Particle density, ρ_s	2650	kg/m^3
Minimum fluidization velocity, U_{mf}	1.70	cm/s
Void fraction at U_{mf}, ϵ_{mf}	0.48	
Bed height at U_{mf}, H_{mf}	10.8–64.5	cm
Fluidization velocity	2–14	cm/s
Reaction kinetic constant	1.57, 0.33	s^{-1}
Other Assumed Parameters		
Sphericity	0.75	
Parameter c in drag formula	0.765	
Parameter d in drag formula	2.928	
Coefficient of restitution	0.8	
Angle of internal friction	30	degree
Fluid viscosity	1.8×10^{-5}	Pa·s
O_3 mass fraction in inlet (O_3–Air) mixture	0.1	

Table 2. Summary of MFIX Equations

Gas continuity

$$\frac{\partial}{\partial t}(\epsilon_g \rho_g) + \nabla\cdot(\epsilon_g \rho_g \boldsymbol{v}_g) = \sum_{n=1}^{N_g} R_{gn}$$

Solids continuity

$$\frac{\partial}{\partial t}(\epsilon_s \rho_s) + \nabla\cdot(\epsilon_s \rho_s \boldsymbol{v}_s) = \sum_{n=1}^{N_s} R_{sn}$$

Species mass balance

$$\frac{\partial}{\partial t}(\epsilon_g \rho_g X_{gn}) + \nabla\cdot(\epsilon_g \rho_g X_{gn} \boldsymbol{v}_g) = R_{gn}$$

Gas momentum

$$\frac{\partial}{\partial t}(\epsilon_s \rho_g \boldsymbol{v}_g) + \nabla\cdot(\epsilon_g \rho_g \boldsymbol{v}_g \boldsymbol{v}_g) = \nabla\cdot\bar{\bar{S}}_g + \epsilon_g \rho_g \boldsymbol{g} - \boldsymbol{I}_{gs}$$

Solids momentum

$$\frac{\partial}{\partial t}(\epsilon_s \rho_s \boldsymbol{v}_s) + \nabla\cdot(\epsilon_s \rho_s \boldsymbol{v}_s \boldsymbol{v}_s) = \nabla\cdot\bar{\bar{S}}_s + \epsilon_s \rho_s \boldsymbol{g} + \boldsymbol{I}_{gs}$$

$$\boldsymbol{I}_{gs} = -\epsilon_s \nabla P_g - F_{gs}(\boldsymbol{v}_s - \boldsymbol{v}_g)$$

Gas–solids drag

$$F_{gs} = \frac{3\epsilon_s \epsilon_g \rho_g}{4 V_{rs}^2 d_p} C_{Ds}\left(\frac{Re_s}{V_{rs}}\right)|\boldsymbol{v}_s - \boldsymbol{v}_g|$$

$$V_{rs} = 0.5\left(A - 0.06Re_s + \sqrt{(0.06Re_s)^2 + 0.12Re_s(2B - A) + A^2}\right)$$

$$A = \epsilon_g^{4.14}, \qquad B = \begin{cases} c\epsilon_g^{1.28} & \text{if} \quad \epsilon_g \le 0.85 \\ \epsilon_g^{d} & \text{if} \quad \epsilon_g > 0.85 \end{cases}$$

Gas-phase stress

$$\bar{\bar{S}}_g = -P_g \bar{\bar{I}} + \bar{\bar{\tau}}_g = -P_g \bar{\bar{I}} + 2\epsilon_g \mu_g \bar{\bar{D}}_g + \epsilon_g \lambda_g tr(\bar{\bar{D}}_g)\bar{\bar{I}}$$

Solids–phase stress

$$\bar{\bar{S}}_s = \begin{cases} -P_s^p \bar{\bar{I}} + \bar{\bar{\tau}}_s^p, & \text{if} \quad \epsilon_g \le \epsilon_g^* \\ -P_s^v \bar{\bar{I}} + \bar{\bar{\tau}}_s^v & \text{if} \quad \epsilon_g > \epsilon_g^* \end{cases}$$

Viscous regime (kinetic theory)

$$P_s^v = K_1 \epsilon_s^2 \Theta_s, \qquad K_1 = 2(1+e)\rho_s g_0, \qquad \bar{\bar{\tau}}_s^v = 2\mu_s^v \bar{\bar{D}}_s + \lambda_s^v tr(\bar{\bar{D}}_s)\bar{\bar{I}}$$

$$\mu_s^v = K_3 \epsilon_s \sqrt{\Theta}_s, \qquad \lambda_s^v = K_2 \epsilon_s \sqrt{\Theta}_s.$$

$$K_3 = \frac{d_p \rho_s}{2}\left\{\frac{\sqrt{\pi}}{3(3-e)}[1 + 0.4(1+e)(3e-1)\epsilon_s g_0] + \frac{8\epsilon_s g_0(1+e)}{5\sqrt{\pi}}\right\}$$

$$\Theta = \left\{\frac{-K_1 \epsilon_s \mathrm{tr}(\bar{\bar{D}}_s) + \sqrt{K_1^2 \epsilon_s^2 tr^2(\bar{\bar{D}}_s) + 4K_4 \epsilon_s [K_2 tr^2(\bar{\bar{D}}_s) + 2K_3 tr(\bar{\bar{D}}_s^2)]}}{2K_4 \epsilon_s}\right\}^2$$

Plastic regime

$$P_s^p = 10^{25}(\epsilon_s - \epsilon_s^{cp})^{10}, \qquad \bar{\bar{\tau}}_s^p = 2\mu_s^p \bar{\bar{D}}_s, \qquad \mu_s^p = P_s^p \sin\phi / 2\sqrt{I_{2D}}$$

$$I_{2D} = ((D_{s11} - D_{s22})^2 + (D_{s22} - D_{s33})^2 + (D_{s33} - D_{s11})^2)/6 + D_{s12}^2 + D_{s23}^2 + D_{s31}^2$$

(Syamlal, 1998a); the value of 30° is typical for sand. The fluid viscosity used is that for air at ambient conditions. A small value of 0.1 was chosen for the O_3 mass fraction at the inlet.

Simulation

The conditions of the Fryer and Potter (1976) experiments were simulated using the MFIX code (Syamlal et al., 1993). The equations solved by this code are based on an interpenetrating fluids formalism of multiphase flow (Anderson and Jackson, 1967). The precise form of the equations and the method of solution are described in detail in MFIX documentation manuals (Syamlal et al., 1993; Syamlal, 1998b). The equations relevant to this simulation are listed in Table 1. These equations represent the conservation of mass and momentum for two interpenetrating phases (gas and catalyst particles) and mass conservation of the gas-phase species (O_2, N_2, and O_3). The stress in the granular phase is described by the kinetic theory of granular material (Lun et al., 1984; Gidaspow, 1994). The granular temperature was calculated using an algebraic closure ("Viscous Regime," Table 2).

The drag law, F_{gs}, which depends on the local slip velocity and void fraction, represents the momentum exchange between the phases. The form used in MFIX is based on exper-

imental correlations of the settling velocity. Such general drag correlations typically can predict the drag force only to an accuracy of about 20% because of the inability to include accurate information about particle size and shape distributions in such correlations. This amount of error is unacceptable in bubbling fluidized-bed simulations. For example, a 5% change in the drag force near minimum fluidization conditions can make a big difference in the fluidization characteristics, which can range from a packed bed to a vigorously bubbling bed with even such a small change in the drag force. Here we propose a method to address this problem, which ensures that the drag force calculated under minimum fluidization conditions exactly matches the experimental drag force. This can be done quite easily, because for any given drag correlation, one can derive an algebraic formula for the minimum fluidization velocity. Here we use such a formula to adjust the parameters c ($=0.765$) and d ($=2.93$) in the formula for B ("Gas-Solids Drag," Table 2) to ensure that the simulated value of U_{mf} corresponded to the reported experimental value of 1.7 cm/s. This ensures that the drag force given by F_{gs} matches the experimental value at the minimum fluidization condition. The correlation is formulated such that the drag force is guaranteed to agree with the single-sphere drag force at the other extreme of very low solids volume. The variation of the drag force with respect to void fraction (albeit modified because B is adjusted) and Reynolds number comes from an experimentally validated Richardson–Zaki-type correlation (Garside and Al-Dibouni, 1977).

The term R_{gn} represents the reaction rate for species n of the gas phase. For this simple kinetics scheme there are three species ($N_g = 3$), only two of which are reactive species; N_2 is included as an inert component. Fryer and Potter (1976) determined that the O_3 decomposition reaction is first order with respect to the O_3 concentration, and have reported rate constants for different catalytic activities. The rate constants, k, were measured in a packed-bed reactor and reported per volume of solid; multiplying their rate expression by ϵ_s converts it to the form used in MFIX, per volume of the reactor, so that

$$R_{O_3} = -\frac{3}{2}R_{O_2} = -\frac{k\epsilon_s \rho_g X_{O_3}}{MW_{O_3}}$$

This set of coupled partial differential equations was solved by MFIX, using a variety of computer platforms (SGI, IBM SP3, Beowulf cluster).

The simulations were performed for a range of conditions reported by Fryer and Potter (1976) assuming two-dimensional (2-D) cylindrical symmetry, initially with a 36×56 (radial $\times$ axial) mesh resolution, corresponding to a computational mesh with $\delta r = 0.318$ cm and $\delta z = 0.536$ cm. We used the second-order accurate Superbee spatial discretization scheme, which is needed to accurately calculate bubble shape (Guenther and Syamlal, 2001). The initial conditions for the simulations were a uniform initial condition, a packed bed. These simulations were repeated at twice the mesh resolution (72×112; $\delta r = 0.159$ cm, $\delta z = 0.268$ cm). All except one of these simulations was started by using the final results of the corresponding coarse-grid simulation as the initial condition. One fine-grid simulation was started from a uniform initial condition, as in the coarse-grid simulations, producing results consistent with the other runs. We thus verified that the results of the fine-grid simulation were insensitive to whether or not the coarse-grid simulation results were used as the initial conditions. Using the coarse-grid solution as an initial condition reduced the simulation time required to eliminate all the initial transients. Numerical results were compared with the reported experimental information by time-averaging the O_3 mass-fraction data for a 10-s period after a statistical steady state was achieved.

Comparison Between Simulation and Experiment

Bed expansion

As a global measure of the degree to which these simulations capture the correct hydrodynamic behavior of the bed, Figure 1 compares the reported percent-bed-expansion data with the calculated values for the three mesh resolutions (36×56, 72×112, and 114×224). This series of simulations was for a fixed initial bed height ($H_{mf} = 11.5$ cm) over a range of superficial velocities ($U_{sup} = 2$, 4, 6, 8, 10, 12, 14 cm/s). Bed height in the experiment was measured by observing "a probe tip from above." Such measurements seem highly subjective, and no error bars were presented. Fryer and Potter (1976) state that the experimental technique "may well underestimate the average bed height" because of the "difficulty of measurement caused by the vigorous motion of the bed." There is no explicit equivalent of this "bed height" in the model results and no unequivocal way to translate the numerical results into a bed height. The void fraction distribution must be postprocessed in some manner to determine this quantity. One way is to time-average the data and then scan downward in the freeboard and mark the first location where the void fraction drops below a certain value—with the idea that the probe tip is visible down to that location. However, this method fails at high fluidization velocities because the upper region of the bed becomes too dilute and may cause the unrealistic prediction of bed contraction. A more realistic way is to calculate the height of the bed that contains a certain percentage of the bed weight. We chose that method because it directly correlates with bed pressure-drop measurements. The bed heights reported by Fryer and Potter perhaps correspond to an (unknown) combination of the two techniques just cited. Therefore, the comparison in Figure 1 is at best semiquantitative.

After a statistical steady state was achieved, we time-averaged the solids distribution; the height that contained 95% of the bed weight was taken as the simulated bed height. The height determined this way was normalized by the value corresponding to 95% of the initial bed height (0.95×11.5 cm). Although this is an arbitrary criterion, the results are not sensitive to the percent bed-weight value chosen (within a small range), because the experimental values are reported as percent bed expansion rather than as actual bed height. For example, using 80% of the bed weight as the criterion made little difference in the simulation results. However, 100% bed weight cannot be used as a criterion, because small amounts of bed material are thrown to high levels. Although the solids volume fraction in the freeboard drops off rapidly with height, the entire freeboard height is required to contain 100% of

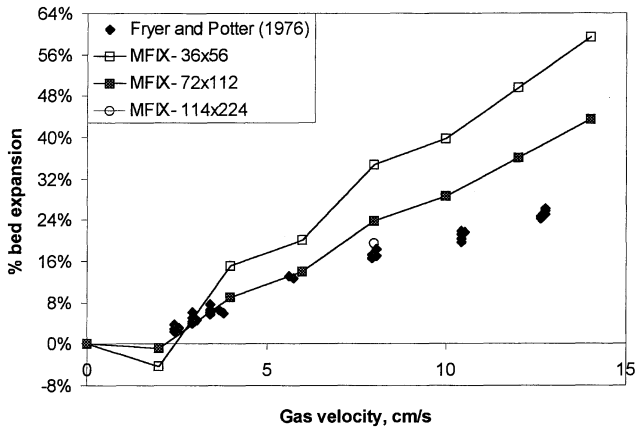

Figure 1. Comparison of calculated bed expansion with data.

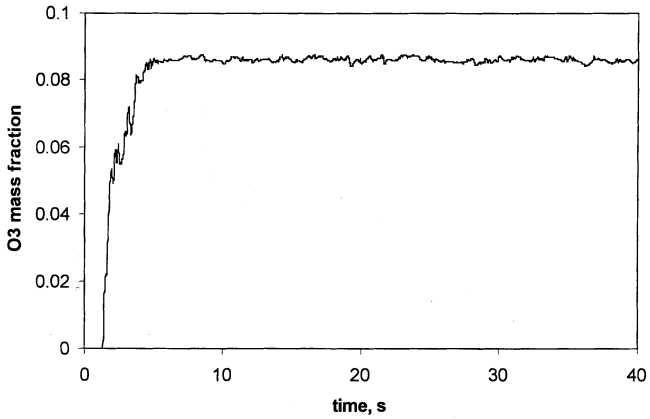

Figure 2. Achieving a statistical steady state in outlet ozone concentration.

the solids. Therefore, the bed height would not change (at the total height of the domain) with gas flow rate, except perhaps at the lowest gas-flow rate.

The solid curves in Figure 1 show simulations at two mesh resolutions. Both simulations show the correct qualitative behavior, expanding from a slumped bed at the minimum fluidization velocity, with expansion slowing at higher fluidization velocity. However, the coarser mesh underestimates bed height at the lowest velocity and significantly overestimates the expansion over the rest of the range. The finer mesh quantitatively tracks the experimental curve (to within the reported reproducibility) up to a superficial velocity of 6 cm/s ($3.5 \times U_{mf}$). The one point calculated using the finest mesh (114×224) (at 8 cm/s) shows improved agreement with the experimental results. The disagreement at higher velocities is partly because of inadequate mesh resolution and partly because of the previously mentioned uncertainty in comparing simulated data with experimental results. Because of this uncertainty and the cost of fine-grid simulation, fine-grid simulations for a range of velocities was not conducted.

Ozone conversion

Since the bed initially contained no O_3, the outlet concentration of O_3 rapidly increases during the first few seconds. This initial transient lasts for 6 to 20 s; the startup lasts longer for deeper beds and lower velocities. After this, the outlet concentration fluctuates around a mean with less than 1% deviation. The average, used to compare with the experimental data, was taken for a 10 s period under these statistically steady conditions. As an example, Figure 2 shows the average outlet concentration of O_3 as a function of time for the simulation at $U = 10.4$ cm/s, $H_{mf} = 10.8$ cm, and $k = 0.33$ m^3-gas/m^3-cat·s. (The units are henceforth abbreviated as s^{-1}; for example, $k = 0.33$ s^{-1}). The initial transients die down after a period of about 10 s, and a statistical steady state is achieved. The standard deviation from 20 to 30 s is very small (0.8%).

Two series of simulations were executed at different mesh resolutions in order to determine the accuracy with which they could duplicate the experimental values reported for total O_3 conversion, C_{out}/C_{in}. This is a global measure of the accuracy of the mathematical description of the chemical process as incorporated into MFIX. The first series was for a fixed initial bed height ($H_{mf} = 11.5$ cm) over a range of superficial velocities ($U = 2, 4, 6, 8, 10, 12, 14$ cm/s). The reported effective rate constants for this bed, as measured by experiments in a packed bed, was $k = 1.57$ s^{-1}.

The results at the lowest mesh resolution (36×56; $\delta r = 0.318$ cm $\times$ $\delta z = 0.536$ cm) are shown in Figure 3 by the curve labeled MFIX-36×56. The simulation at this level of resolution shows reasonable agreement with the experiments, predicting the shape of the curve and the general trend. However, the outlet concentration is significantly underpredicted.

The simulations were repeated at twice the mesh resolution (72×112; $\delta r = 0.159$ cm, $\delta z = 0.268$ cm). All except one of these simulations (at $U = 8$ cm/s) were started by using the final results of the corresponding coarse-grid simulation as the initial condition. At this mesh resolution, the simulation results for conversion agree quantitatively with those reported experimentally over the full range of superficial velocities studied. (See the curve labeled MFIX-72×112 in Figure 3.) In order to firmly establish the mesh independence of these simulations for this global experimental measurement, a simulation was repeated at one superficial velocity ($U = 8$ cm/s) at an even higher resolution (144×224; $\delta r = 0.0795$ cm,

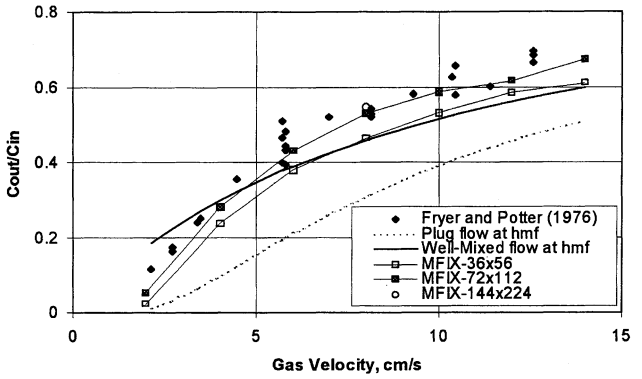

Figure 3. Outlet mass fraction of ozone as a function of gas velocity ($H_{mf} = 11.5$ cm; $k = 1.57$ s^{-1}).

$\delta z = 0.134$ cm). Only a slight change in the calculated conversion value occurred for this point, shown as MFIX-144$\times$244 in Figure 3. Thus, based on the results shown in Figures 1 and 3, the solution for 72×112 appears to be grid independent. These criteria used for judging grid independence, bed expansion, and total conversion, are global measures of the hydrodynamic and chemical behavior of the bed. This is a necessary first step, from which we can conclude that the full solution is reasonably grid independent.

The presence of a solids volume fraction in the rate expression couples the hydrodynamics and the chemical reactions. To determine how strong an influence hydrodynamics has on the chemical reactions, we have plotted the results of two simple models that idealize gas–solids hydrodynamics in a fluidized bed: a plug-flow reactor and a well-mixed reactor. Formulas for conversion in plug-flow and well-mixed reactors are derived (ignoring the volume change caused by the reaction, about 3%) as follows

Plug flow

$$\frac{\left[X_{O_3}\right]_{\text{outlet}}}{\left[X_{O_3}\right]_{\text{inlet}}} = \exp\left(-k\epsilon_s H_{mf}/U\right)$$

Well-mixed

$$\frac{\left[X_{O_3}\right]_{\text{outlet}}}{\left[X_{O_3}\right]_{\text{inlet}}} = \frac{1}{1+\left(k\epsilon_s H_{mf}/U\right)}$$

where H_{mf} is the bed height at minimum fluidization, and U is the fluidization velocity. (We purposely use H_{mf} rather than the actual bed height to avoid having to include any information based on bed hydrodynamics in this model; the actual bed height, defined in some manner, would have to be obtained from experimental data.) We want to demonstrate that such models, which idealize bed hydrodynamics, cannot predict the observed conversion as a function of gas velocity. This in turn implies that hydrodynamics affect the chemical reaction and that the experimental data are useful for validating the model's ability to capture the influence of hydrodynamics on chemical reactions. There are other models that include other hydrodynamic information (bubble size, rise velocity, wake fraction, and so on) that can easily describe the observed reactor behavior [for example, Fryer and Potter (1976)]. The advantage of the present model is that it requires only one (easily measured) hydrodynamic parameter—minimum fluidization velocity—to calibrate the drag correlation.

Figure 3 shows that at the minimum fluidization velocity, the experimental data and the results of the simulation are similar to the plug-flow reactor, which is to be expected because the solids are not moving. At higher velocities, the outlet concentration (experimental and predicted) steadily becomes greater than that of a plug-flow reactor. Perhaps the gas mixing induced by the bubbles causes this, which suggests the usage of a well-mixed reactor model to describe the fluidized bed. Figure 3 shows that to some extent the well-mixed reactor describes the fluidized-bed reactor. At low velocities the outlet concentration is lower than that in a well-mixed reactor; as the velocity is increased, the outlet concentration becomes closer to that of a well-mixed reactor. Surprisingly, at velocities larger than 5 cm/s ($\sim 3U_{mf}$) the conversion in the fluidized-bed reactor is worse than that in a well-mixed reactor. The higher outlet concentration (or lower conversion) is because of the gas bypassing the catalyst bed through bubbles. MFIX predicts this transition remarkably well.

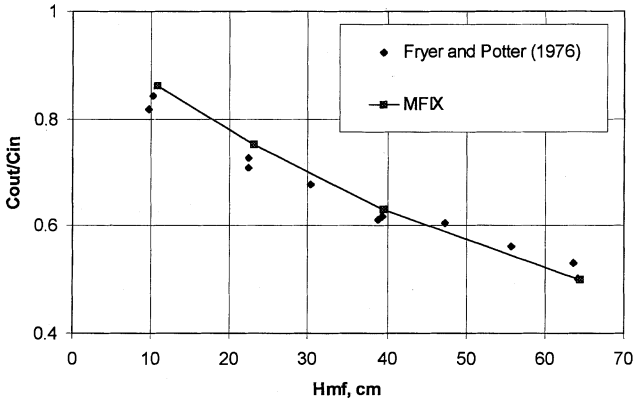

Figure 4. Conversion as a function of initial bed height at $U = 10$ cm/s and $k = 0.33$ s^{-1}.

A second series of simulations was conducted for a fixed-fluidization velocity ($U = 10.4$ cm/s) over a range of bed heights ($H_{mf} = 10.8$, 23.1, 39.5, 64.5 cm). The reported effective rate constant for this bed, as measured by experiments in a packed bed, was $k = 0.33$ s^{-1}. The grid size was held constant at $\delta r = 0.159$ cm and $\delta z = 0.268$ cm, which corresponds to the resolution (72×112) that gave a grid-independent solution in the first series of simulations. Figure 4 shows the outlet O_3 concentration as a function of bed height. The simulation results agree with experimental data very well over the entire range of initial bed heights.

We saw that the calculated outlet O_3 concentration agrees remarkably well with experimental data without any need for adjustable constants. To further validate the hydrodynamic model, we compared detailed profiles of field variables in the model. Such data are often difficult to measure. Fortunately, Fryer and Potter gave axial profiles of O_3 concentration. In Figure 5, we compare those data with calculated profiles for $H_{mf} = 23.1$ cm, $U = 10.4$ cm/s, and $k = 0.331$ s^{-1}.

Fryer and Potter measured the O_3 concentrations at four (unstated) radial locations in the bed and reported an average value. To mimic the experimental technique, we sampled the concentration at four radial locations in the bed, 0.2, 3.8, 7.6, and 11.3 cm from the center line, and obtained an average from these four values. Experiments showed that "concentrations detected by four probes across any one radius do not differ significantly in comparison with axial variations." The simulation results for the region near the top of the bed agree with this observation. In the bottom part of the bed, however, the simulation results show significant variation in the radial direction.

A remarkable feature of the experimental data is that the concentration reaches a minimum value in the bed. This was consistently observed in the experiments for fluidization velocities above 5.8 cm/s. Fryer and Potter (1976) give reasons to justify that this is a real phenomenon rather than an arti-

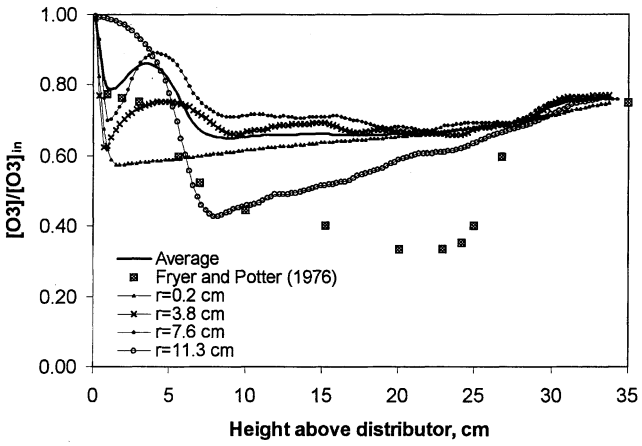

Figure 5. Average axial concentration of ozone at H_{mf} = 23.1 cm, U = 10.4 cm/s, and k = 0.331 s^{-1}.

fact caused by sampling. The simulation curve shows a minimum, but one that is significantly less pronounced and occurs much deeper in the bed than in the experimental data. (The data point for $H = 35$ cm shown in Figure 5 was not included in the profile data, but was reported separately as outlet concentration by Fryer and Potter.) Although there is good agreement between the experimental and calculated outlet concentrations, there is considerable deviation in the axial concentration profiles. We cannot assess the reasons for this discrepancy, however, without error estimates for the experimental radial profiles.

Comparisons with plug-flow and stirred-tank reactors show that reactor hydrodynamics critically affect overall conversion. To understand how this occurs, we examined the instantaneous behavior of the bed. Figure 6 shows the instantaneous ($t = 13.8$ s) void-fraction and species mass-fraction distributions with superimposed gas and solids velocity vectors for $H_{mf} = 11.5$ cm, $U = 8$ cm/s, and $k = 1.57$ s^{-1}. The results plotted are for 2-D axisymmetric simulation. In each of the plots, the left edge is the center line and the right edge is the outside wall.

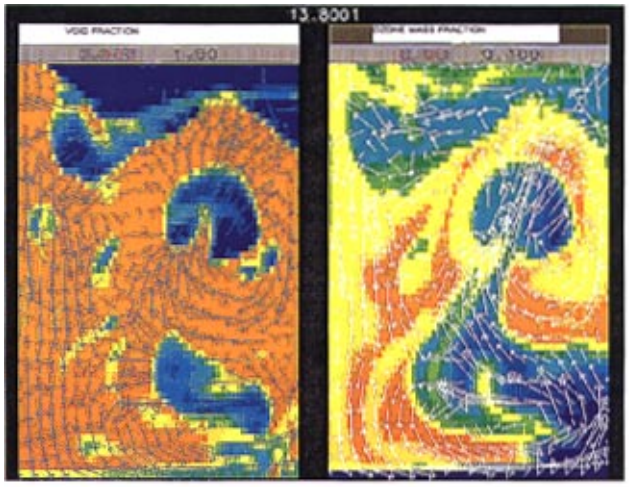

Figure 6. Void fraction and mass-fraction distributions and velocity vectors.

The left panel of Figure 6 shows the voidage as a color plot. The color scale varies from 0.4 (red) to 1 (blue). Superimposed on this panel are the solids velocity vectors; for clarity, only one in nine of the calculated vectors is plotted. The right panel shows the O_3 mass fraction on a color scale 0 (red) to 0.1 (blue). The gas velocity vectors are superimposed on this panel. The bubble rise path determines the flow pattern in the bed.

In general, the simulations show a narrow region near the distributor (which is simulated as a uniform-flow boundary condition), with a layer of an expanded bed. Slightly above the distributor, this band rolls up into a bubble, which usually initially forms near the outside lower edge of the bed. Once formed, these bubbles rise and migrate toward the center line of the bed. On average, this generates a sloping band of reduced voids from the lower outside region of the vessel toward the center line. This is a band of high gas flow, related to gas bypassing the bed in the "bubble phase." The bubble-induced time-averaged solids motion shows a downward circulation pattern near the center line, and there is also downward flow of solids near the outside wall near the top of the bed. The bed is not deep enough to establish an upward solids circulation pattern near the center line; bubbles do not have enough time to migrate completely to the center of the bed before bursting at the surface. This type of pattern is typical of shallow bubbling beds.

In the void fraction plot (left panel), a bubble close to the top of the bed is visible. The O_3 mass-fraction plot is quite similar to the void-fraction plot: in high void-fraction regions, the O_3 concentration is high and vice versa. This is because the rate of O_3 decomposition is proportional to the solids volume fraction. However, there is a significant deviation from this trend within a region in the bubble wake. Interestingly, the O_3 mass fraction is high in a region where the void fraction is low. The low conversion in that region appears to be because of the high gas flow rate: a gas jet is flowing from the bottom bubble to the top bubble. So gas bypassing is caused by the gas flowing through the bed as a bubble, and the gas flowing from bubble to bubble in the form of jets.

The vector plots also show that the gas and solids flow patterns are quite alike. This is because of the small particle size and the consequent large drag force. In certain regions of the bed, the gas flow is downward, especially near the bed center line. Even bubbles caught in this region move downward. This reverse flow of gas has been used to explain the minimum observed in the axial concentration profile shown in Figure 5 (Peters et al., 1982). At sufficiently high downward solids velocity in the emulsion phase, the gas flow will reverse direction in order to maintain a constant relative velocity to the solids.

Figures 7 and 8 show the time-averaged void fraction and velocity vectors for two initial-bed heights. The gas–solids circulation pattern predicted by the simulation is similar to those reported for a shallow bed (Kuni and Levenspiel, 1991; Werther and Molerus, 1973): up at the wall, down near the center line. Figure 7a presents the time-averaged solids-velocity vectors, superimposed on contour lines representing the time-averaged void fraction (blue represents a void fraction of 1 (as in the freeboard, for example) and red represents a void fraction of 0.4). A similar representation of the time-averaged gas velocity is shown in Figure 7b. The results

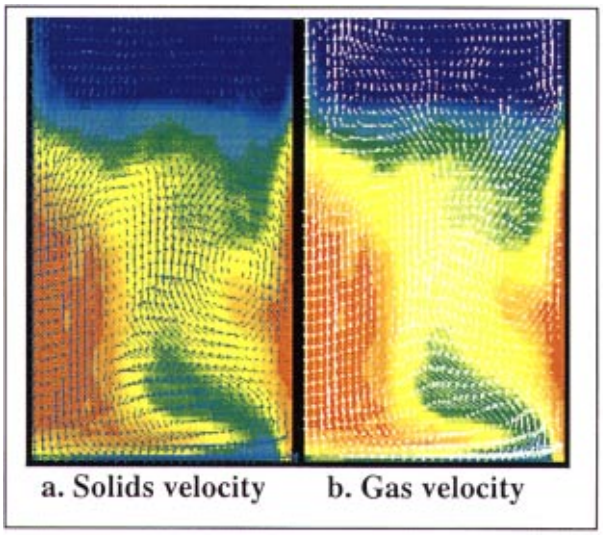

Figure 7. Time-averaged velocity vectors and contours of void fraction ($U = 10$ cm/s; $H_{mf} = 11.5$ cm).

plotted are for 2-D axisymmetric simulation. As before, in each of the plots, Figures 7a and 7b, the left edge is the center line and the right edge is the outside wall.

The overall solid circulation pattern observed in the simulation was, up at the outside, and down on the center line. However, there was much more detail to the pattern than is generally described in the literature. There is a uniform low-voidage region very close to the distributor, because of the uniform constant boundary condition imposed to simulate the distributor. (No attempt was made to resolve the detailed geometry of the bubble-cap distributor used experimentally.) However, this region was unstable and rolled up in a region near the outside wall to form "bubbles."

It is not clear why the instability is stronger near the wall, but this prediction agrees with the experimentally reported behavior: bubbles preferentially form near the junction of the distributor and the outside wall (Werther and Molerus, 1973). These bubbles then rose rapidly through the bed, while migrating toward the center line. However, since the simulated bed was quite shallow, the migration to the center line was never complete. This general route of bubble motion, of course, results in a solids motion of the same pattern. This upward motion induced a downward flow of particles near the center line, which diverted to the outside near the distributor. This particle flow was often strong enough to cause downward flow of the entrained gas in this region. There was also a small reverse circulation pattern of solids in the upper outside region of the bed, caused by the migration of the bubbles toward the center line. Of course, this pattern was more pronounced for the deeper beds.

In Figure 8, the superficial velocity is the same as that shown in Figure 7, or 10.4 cm/s; however, the initial bed height has been increased to 23.1 cm. The downflow region near the center becomes smaller higher up in the bed, and the reverse circulation pattern in the upper outside corner has intensified. It is this pattern that would presumably grow to establish the second circulation cell characteristic of deeper beds: up at the center line; down at the wall.

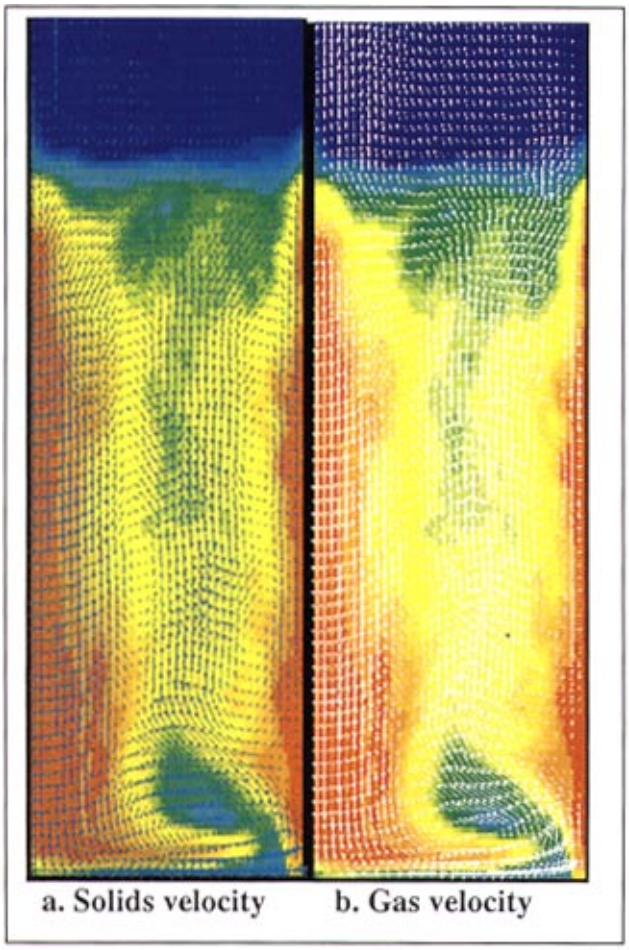

Figure 8. Time-averaged velocity vectors and contours of void fraction ($U = 10.4$ cm/s; $H_{mf} = 23.1$ cm).

In this article we have reported the results of 2-D axisymmetric simulations. Although the time-averaged profiles must be axisymmetric, the validity of this approximation in transient simulations is not established. Also, we are not sure whether this approximation may have prevented the bubbles from moving to the center in the 23.1-cm-tall bed (Figure 8). Therefore, we have started an investigation using a three-dimensional (3-D) geometry. However, 3-D simulations are very slow and time-consuming; results will be reported in a future publication.

Conclusions

A gas–solids flow model was used in this study to model a catalytic reaction—the decomposition of O_3 with an iron oxide catalyst—in a bubbling fluidized bed. By using three-grid resolutions (36×56, 72×112, and 114×224), we show that a grid-independent solution can be obtained that agrees very well with the observed O_3 outlet concentration as a function of fluidization velocity and initial bed height. The agreement in the bed expansion was good at low fluidization velocities, but not as good at high fluidization velocities. However, Fryer and Potter noted an uncertainty in determining bed height at

high fluidization velocities. The axial variation in O_3 concentration (cross-section averaged) shows a minimum within the bed, as observed in the experimental data. However, the location and magnitude of the minimum are considerably different from experimental data.

The instantaneous solids circulation and solids distribution patterns agree qualitatively with general observations in fluidized beds. The calculations show that gas may bypass the bed by jetting between bubbles. The time-averaged void-fraction plots show bubble formation near the wall and migration toward the center. However, bubbles do not reach the center, perhaps because of (1) the short bed heights considered in these simulations, or (2) a limitation of the 2-D axisymmetric assumption used in these simulations. We plan to conduct 3-D simulations to verify this. In summary, the gas–solids multiphase flow model used here is able to capture the effect of gas–solids hydrodynamics on catalytic reactions in a bubbling fluidized bed remarkably well without using any adjustable constants.

Acknowledgments

This work was supported by funding from U.S DOE–Fossil Energy, National Energy Technology Center, and U.S DOE–Energy Efficiency and Renewable Energy, Office of Industrial Technologies. The authors thank the EERE-OIT program manager, Dr. Brian Valentine, for his support.

Literature Cited

Anderson, T. B., and R. Jackson, "A Fluid Mechanical Description of Fluidized Beds," *Ind. Eng. Chem. Fundam.*, **6**, 527 (1967).

Boemer, A., H. Qi, and U. Renz, "Verification of Eulerian Simulation of Spontaneous Bubble Formation in a Fluidized Bed," *Chem. Eng. Sci.*, **53**, 1835 (1998).

Bukur, D. B., "Analysis of Gas Flow in Fluidized-Bed Reactors," *Ind. Eng. Chem. Fundam.*, **17**, 120 (1978).

Fryer, C., and O. E. Potter, "Countercurrent Backmixing Model for Fluidized Bed Catalytic Reactors. Applicability of Simplified Solutions," *Ind. Eng. Chem. Fundam*, **11**, 338 (1972).

Fryer, C., and O. E. Potter, "Experimental Investigation of Models for Fluidized Bed Catalytic Reactors," *AIChE J.*, **22**, 38 (1976).

Frye, C. G., W. C. Lake, and H. C. Eckstrom, "Gas-Solid Contacting with Ozone Decomposition Reaction," *AIChE J.*, **4**, 403 (1958).

Garside, J., and M. R. Al-Dibouni, "Velocity-Voidage Relationships for Fluidization and Sedimentation in Solid-Liquid Systems," *Ind. Eng. Chem. Process Design Dev.*, **16**(2), 206 (1977).

Gidaspow, D., *Multiphase Flow and Fluidization: Continuum and Kinetic Theory Descriptions*, Academic Press, New York (1994).

Gidaspow, D., and A. Therdthianwong, "Hydrodynamics & SO_2 Sorption in a CFB Loop," *Proc. Int. Conf. on Circulating Fluidized Beds*, Somerset, PA, p. 351 (1993).

Guenther, C., and M. Syamlal, "The Effect of Numerical Diffusion on Simulation of Isolated Bubbles in a Gas-Solid Fluidized Bed," *Powder Technol.*, **116**, 142 (2001).

Heimerl, J. M., and T. P. Coffee, "The Detailed Modeling of Premixed, Laminar Steady-State Flames I. Ozone," *Combust. & Flame*, **39**, 301 (1980).

Hovmand, S., W. Freedman, and J. F. Davidson, "Chemical Reaction in a Pilot-Scale Fluidized Bed," *Trans. Inst. Chem. Eng.*, **49**, 149 (1971).

Kuipers, J. A. M., K. J. Van Duin, F. P. H. Van Beckum, and W. P. M. Van Swaaij, "A Numerical Model of Gas Fluidized Beds," *Chem. Eng. Sci.*, **47** (8), 1913 (1992).

Kunii, D., and O. Levenspiel, *Fluidization Engineering*, 2nd ed., Butterworth-Heinemann, Boston (1991).

Lun, C., S. Savage, D. Jeffrey, and N. Chepurniy, "Kinetic Theories for Granular Flow: Inelastic Particles in Couette Flow and Slightly Elastic Particles in a General Flowfield," *J. Fluid Mech.*, **140**, 223 (1984).

Orcutt, J. C., J. F. Davidson, and R. L. Pigford, "Reaction Time Distribution in Fluidized Catalytic Reactors," *Chem. Eng. Prog. Symp. Ser., No. 38*, **58**, 1 (1962).

Ouyang, S. J., J. Lin, and O. E. Potter, "Ozone Decomposition in a 0.254 m Diameter Circulating Fluidized Bed Reactor," *Powder Technol.*, **74**, 73 (1993).

Peters, M. H., L.-S. Fan, and T. L. Sweeney, "Reactant Dynamics in Catalytic Fluidized Bed Reactors with Flow Reversal of Gas in the Emulsion Phase," *Chem. Eng. Sci.*, **37**, 553 (1982).

Samuelsberg, A., and B. H. Hjertager, "Simulation of Two-Phase Gas/Particle Flow and Ozone Decompositions in a 0.25m I.D. Riser," *Advances in Multiphase Flow*, A. Serizawa, T. Fukano, and J. Batalille, eds., Elsevier Science B.V., Amsterdam, The Netherlands, p. 679 (1995).

Syamlal, M., "Higher Order Discretization Methods for the Numerical Simulation of Fluidized Beds," *Fluid. Fluid Part. Syst.: Recent Res. and Dev.*, *AIChE Symposium Series*, **94**, 138 (1998a).

Syamlal, M., *MFIX Documentation: Numerical Technique*, NTIS Report No. DE-AC21-95 MC 31346, Springfield, VA (1998b).

Syamlal, M., and T. J. O'Brien, "Computer Simulations of Bubbles in a Fluidized Bed," *AIChE Symp. Ser.: Fluidization, Fluid Particle System Fundamentals Applied*, **85**, 22 (1985).

Syamlal, M., W. Rogers, and T. O'Brien, *MFIX Documentation: Theory Guide*, Tech. Note, NTIS Report No. DOE/METC-94/1004 (DE94000087), Springfield, VA, (also, see www.mfix.org) (1993).

Theologos, K. N., and N. C. Markatos, "Advanced Modeling of Fluid Catalytic Cracking Riser-Type Reactors," *AIChE J.*, **39**, 1007 (1993).

Van Deemter, J. J., "Mixing and Contacting in Gas-Solid Fluidized Beds," *Chem. Eng. Sci.*, **13**, 143 (1961).

Van Swaaij, W. P. M., and F. J. Zuiderweg, "Investigation of Ozone Decomposition in Fluidized Beds on the Basis of a Two-phase Model," *Proc. Eur. Symp. on Chemical Reaction Engineering*, Amsterdam, The Netherlands (1972).

Van Wachem, B. G. M., J. C. Schouten, R. Krishna, and C. M. van den Bleek, "Eulerian Simulations of Bubbling Behavior in Gas-Solid Fluidized Beds," *Comput. Chem. Eng.*, **22** (Suppl.), S299 (1998).

Van Wachem, B. G. M., J. C. Schouten, C. M. van den Bleek, R. Krishna, and J. L. Sinclair, "Comparative Analysis of CFD Models of Dense Gas-Solid Systems," *AIChE J.*, **47**, 1035 (2001).

Werther, J., and O. Molerus, "The Local Structure of Gas Fluidized Beds—II. The Spatial Distribution of Bubbles," *Int. J. Multiphase Flow*, **1**, 123 (1973).

Manuscript received July 11, 2002, and revision received Apr. 3, 2003.